Plasma Phys. Control. Fusion **50** (2008) 124054 (13pp) doi:10.1088/0741-3335/50/12/124054

Recent progress in understanding the behavior of dust in fusion devices

S I Krasheninnikov[1], A Yu Pigarov[1], R D Smirnov[1], M Rosenberg[1], Y Tanaka[2], D J Benson[1], T K Soboleva[3], T D Rognlien[4], D A Mendis[1], B D Bray[5], D L Rudakov[1], J H Yu[1], W P West[5], A L Roquemore[6], C H Skinner[6], J L Terry[7], B Lipschultz[7], A Bader[7], R S Granetz[7], C S Pitcher[8], N Ohno[9], S Takamura[9], S Masuzaki[10], N Ashikawa[10], M Shiratani[11], M Tokitani[10], R Kumazawa[10], N Asakura[12], T Nakano[12], A M Litnovsky[13], R Maqueda[14] and the LHD Experimental Group

[1] University of California at San Diego, La Jolla, CA, USA
[2] Kanazawa University, Kanazawa, Japan
[3] ICN, Universidad Nacional Autónoma de México, México D. F., México
[4] Lawrence Livermore National Laboratory, Livermore, CA, USA
[5] General Atomics, San Diego, CA, USA
[6] Princeton Plasma Physics Laboratory, Princeton, NJ, USA
[7] PSFC, Massachusetts Institute of Technology, Cambridge, MA, USA
[8] ITER Cadarache Joint Work Site, Cedex, France
[9] Graduate School of Engineering, Nagoya University, Nagoya, Japan
[10] National Institute for Fusion Science, Toki, Japan
[11] Department of Electronics, Kyushu University, Fukuoka, Japan
[12] Naka Fusion Institute, JAEA, Naka, Japan
[13] Institut für Energieforschung-Plasmaphysik FZ Jülich, Jülich, Germany
[14] Nova Photonics, Princeton, NJ, USA

Received 12 May 2008, in final form 24 July 2008
Published 6 November 2008
Online at stacks.iop.org/PPCF/50/124054

Abstract

It has been known for a long time that microscopic dust appears in plasmas in fusion devices. Recently it was shown that dust can be responsible for the termination of long- discharges. Also, in ITER-scale experiments dust can pose safety problems related to its chemical activity, tritium retention and radioactive content. In particular, the presence of dust in the vacuum chamber of ITER is one of the main concerns of the ITER licensing process. Here we review recent progress in the understanding of different experimental and theoretical aspects of the physics of dust dynamics and transport in fusion plasmas and discuss the remaining issues.

(Some figures in this article are in colour only in the electronic version)

1. Introduction

It has been known for a long time that microscopic grains of solid matter (dust) appear in plasmas in fusion devices. Previous reviews of dust issues in fusion plasma including the analysis of collected dust as well as the discussions of possible mechanisms of dust generations and safety issues associated with dust can be found in [1–5].

One of the reasons why a lot of attention has recently been directed to the study of dust is the safety issue of ITER-scale experiments: dust can pose safety problems related to its chemical activity, tritium retention and radioactive content. In particular, the presence of dust in the vacuum chamber of ITER is one of the main concerns of the ITER licensing process [6]. Another important dust-related issue for ITER is 'to avoid degradation of in-vessel diagnostic components, such as mirrors, due to dust, material deposition and erosion' [7].

For ITER, there are two basic safety limits [8] which must be observed, one related to hot dust (higher than 400 $^\circ$ C for Be and W and above 600 $^\circ$ C for C) and another related to cold dust. The hot dust accident scenario assumes simultaneous water and air leaks. The water reacts with the hot dust, producing hydrogen gas, which would then react with oxygen, producing an explosion. This sets the limits of dust. We notice that the tungsten limit is large compared with Be and C. This, combined with the relatively low erosion rate expected for tungsten, probably means hot tungsten is not an issue in ITER. The accident scenario associated with the cold dust limit assumes a vacuum vessel penetration (e.g. window breaking) and a small quantity (tens of grams) of in-vessel activated dust escaping the primary containment. The limit is determined by the radiological nature of the activated W, Be and C, the size of the ITER site and the distance to the nearest residential areas. Both Be and C are relatively innocuous compared with radioactive W, and so the cold dust limit is a tungsten dust limit.

However, in addition to all of that, very recent experiments clearly show that the termination of long pulse discharges on the LHD stellarator is caused by the entrance into the core region of large dust particles coming from the wall [9]. Therefore, it is plausible that dust can play an important role in the performance of fusion devices in 'standard' regimes as well. On the other hand, it is also conceivable that dust can be used in fusion plasmas for some useful purposes (e.g. diagnostics).

In this paper we review recent progress in the understanding of different aspects of the physics of dust dynamics and transport in fusion plasmas and discuss the remaining issues. Such topics as dust generation mechanisms and dust removal techniques are beyond the scope of this paper.

2. Experimental study of dust in fusion plasmas

At present the majority of available data on dust in fusion plasmas are obtained with: (a) dust collection during the vents and analysis of this dust [1, 2, 4, 5, 10–15], (b) laser scattering technique [16–18] and (c) fast cameras (e.g. see [3, 9, 19–23]).

Among other diagnostics developed recently for dust study in fusion plasmas are electrostatic detectors [24], which are based on the 'grilling' of dust particles when they fall on two closely interlocking grids of wires, and capacitive diaphragm microbalance [25], which is based on pressure gauge technology.

Collection of dust. Dust collections followed by analysis of collected material from the main chamber walls has become a common procedure in many tokamaks [1–5, 10–15]. The typical size, composition, morphology and surface distribution of the collected dust have been studied. The studies show that the sizes of fusion dust vary in a very wide range from tens of

nanometers to hundreds of micrometers. The collected dust typically consists of the chamber wall's materials and has a variety of flake-like, irregular and, sometimes, spherical shapes, which suggest different mechanisms of dust production. Among the mechanisms considered are flaking of deposited layers, condensation of impurities in cold plasma regions, sputtering of plasma contacting surfaces and other surface damage mechanisms such as brittle destruction, melting and unipolar arcs (e.g. see [1–3, 5]).

The amount of dust collected in tokamaks depends on the history of the plasma parameters in the discharges and the overall duration of plasma operations since the surfaces were last cleaned. Estimates of the total dust inventory, the particle size distribution and the composition can be found in [2, 4, 10–15]. They show that the total dust inventory ranges from 0.5 g (NSTX) to 90–120 g (DIII-D). The surface mass density ranges from 0.03 g m^{-2} (NSTX) to 10 g m^{-2} (C-Mod). The particle sizes (measured by analysis of optical and scanning electron microscope and transmission electron microscope images of the dust) most often follow a log normal distribution. The count median diameter ranges from 0.46 μm (DIII-D) to 9.6 μm (LHD). Note that particles smaller than the 0.02 μm pores of the filters used to vacuum up the dust are not collected or included in the above estimates. In particular, nano-scale particles have been observed in Tore Supra [26] and TEXTOR [1]. The effective surface area, measured by the Brunauer–Emmett–Teller technique, is of the order of a few m^2 g^{-1}.

In ITER a direct global dust inventory measurement by the collection of dust will be very difficult, if not impossible. Therefore, a simple and conservative approach is planned which assumes the dust inventory is proportional to the net eroded materials, i.e. dust $=$ $f_{\rm dust} \times$ (net erosion), where at this moment it is assumed that $f_{\rm dust} = 1$ (although some current experiments suggest that $f_{\rm dust}$ can be significantly smaller than one, e.g. $f_{\rm dust} \approx 0.1$ [27]).

Observations of dust by laser scattering. The non-shifted detector channels of the Thomson scattering system can be used for the studies of dust statistics in the plasma [16–18]. Because of the short laser pulse duration and small viewing volume dust observation rates are low, a few events per discharge or less. The interpretation of experimental data also has some complications [28] related to: (a) partial or even complete ablation of the dust grain by the laser beam (which usually has an energy $\sim$1 J) and (b) comparable values of the laser wavelength and the size of the dust grain, which requires one to use the more complex Mie scattering model rather than simple Rayleigh approximation.

A more accurate analysis of the DIII-D data using the Mie scattering model and taking account of the particle ablation by the laser has put the detectable particle size within the range 0.16–1.6 μm in diameter [29]. The densities of sub-micrometer dust particles, inferred from the laser scattering data, in both the upper scrape-off layer (SOL) and the lower divertor regions are shown in figure 1 [18].

The probability distribution functions (PDFs) over the radius, $R_{\rm d}$, of experimentally detected dust particles in DIII-D were constructed from a fit to the scattering signal distribution obtained over 710 discharges comprising 1580 dust events [18] assuming graphite particles with complex index of refraction $m = 3.33 - i2.07$ [29]. The PDF can be fitted rather well with the power-law function, $R_{\rm d}^{-\sigma}$, where $\sigma \sim 2.7207$ [29]. Such PDF formally causes the divergence of total mass of dust at $R_{\rm d} \to \infty$. Therefore, it suggests that the contributions of large particles ($R_{\rm d} \gtrsim 10\,\mu$m, which are missed in these laser scattering measurements) in both impurity content and plasma contamination may be crucial.

Observations of dust with fast cameras. As we already mentioned before, one of the early observations of small objects flying in fusion plasma was done with a film camera [30].

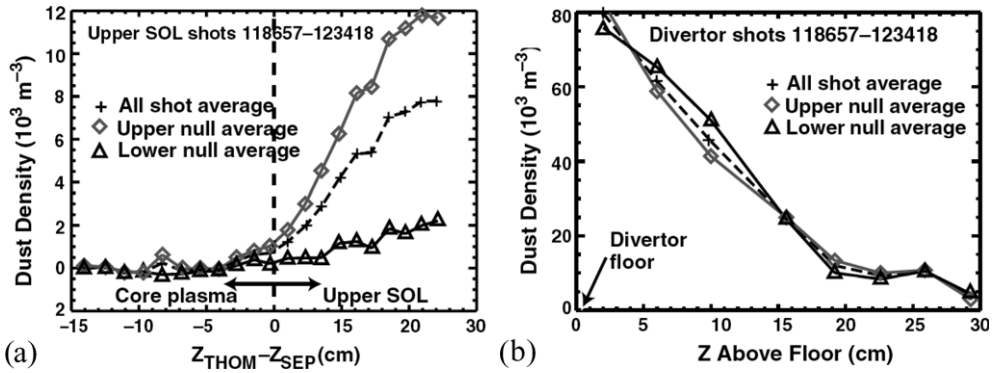

Figure 1. The dust grain densities as a function of distance along the laser path for (*a*) the upper SOL (density is referenced to the average location of the separatrix over all times searched) and (*b*) the lower divertor (distance is referenced to the divertor strike plate) [18].

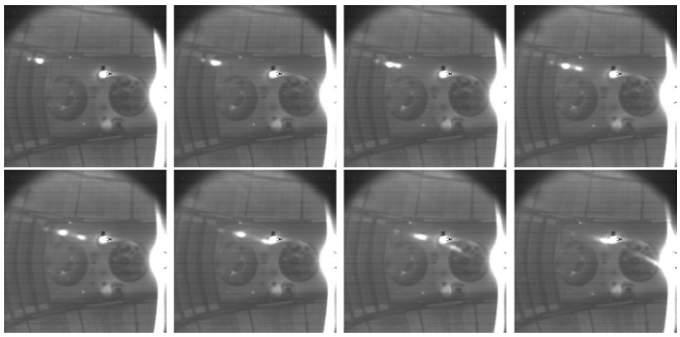

Figure 2. Motion of a dust particle in the NSTX.

Today, fast-framing cameras are widely used to monitor different phenomena occurring in edge plasmas (e.g. blobs, ELMs) also including the dust particles (e.g. see [3, 9, 19–23]). In addition to the detection of the dust, fast cameras are used to estimate the speed of dust grains. The tracking of a dust particle with a few fast cameras and measurements of the radiation spectrum can provide important information on both dust properties and plasma parameters. Tracking of dust with two cameras with subsequent numerical simulation trajectories of particles were performed on NSTX and quantitative agreement between the simulated and experimentally observed trajectories was found [21].

As an example, a sequence of frames in figure 2 shows a dust particle that first becomes visible in the outboard SOL in NSTX, then moves across the screen and splits into two smaller particles. The total time between the first and the last frames is ∼5 ms, which gives the speed of the particle ∼150 m s^{-1}.

One of the complications with the interpretation of the visible images of natural dust in fusion plasmas is the lack of knowledge about dust's shape, composition, size, etc. Therefore, the monitoring of well-characterized dust deliberately injected into fusion plasma can significantly simplify the data analysis, help to benchmark theoretical models and can even serve as a diagnostic tool. So far, only a few such experiments have been performed [16, 22, 23]. On DIII-D ∼30 mg of carbon dust with diameter ∼1–15 μm was placed on a DiMES sample holder and was exposed to high-power LSN ELMing H-mode discharges with strike points

swept across the divertor floor [22]. Individual dust particles were observed with a TV camera moving at velocities of $\sim$100 m s^{-1}, predominantly in the toroidal direction, consistent with the ion drag force. About 1.5–2% of the total dust carbon content ((2–3) $\times$ 10^{19} carbon atoms, equivalent to a few million dust particles) penetrated the core plasma, raising the core carbon density by a factor of 2–3 and resulting in a twofold increase in the total radiated power.

Observation of dust 'statistics' with the cameras on DIII-D shows that during 'normal operations', i.e. when the vacuum vessel walls are well conditioned and there are no major disruptions, dust observation rates are low. Standard cameras register only isolated dust events, single numbers per discharge or none, while the fast camera typically observes between 10 and 100 events per discharge. Individual particles moving at velocities of up to $\sim$500 m s^{-1} and collisions of particles with the walls as well as breakup of larger particles into pieces are observed. The preferential direction of dust motion is toroidal, however, in some cases the trajectories of dust grains are very surprising. Disruptions often generate significant amounts of dust (up to $\sim$10 000 dust particles), which is directly observed by the fast-framing camera. Increased dust levels are also observed following entry vents. In the first 2–3 plasma discharges after an entry vent, standard rate cameras detect hundreds of particles and fast camera detects thousands of particles in each discharge. After about 15 discharges dust is virtually gone during the stationary portion of a discharge, and appears at much reduced levels during the plasma initiation and termination phases. After a few days of plasma operations (about 70 discharges) dust levels are further reduced to the 'normal operations' rates. Similar trends in dust trajectories and statistics as well as the 'self-cleaning' of plasma from dust were shown on many magnetic fusion devices. In particular, in Alcator C-Mod, only $\sim$20 run hours were needed for recovery after major failure of the low-hybrid wave launcher, which caused a rain of dust [31].

However, it is obvious that the 'self-cleaning' of plasma from dust is not necessarily possible within one shot. Moreover, deliberate or accidental injection of a large amount of dust can result in the termination of the discharge. As an example of such a scenario, in figure 3 one can see the termination of a long pulse discharge in LHD caused by the 'spark' event resulting in accidental injection of a large amount of the iron containing dust into plasma [9]. The 'spark' was triggered by a local overheating of the first wall. Similar scenarios were observed on other devices in both regular and long pulse discharges.

In most fusion devices the estimate of typical speed of dust grains observed with fast cameras is within a few $\times$ 100 m s^{-1}. However, some plausible interpretation of experimental data from the FTU tokamak suggests the presence of dust grains moving with a very high speed $\sim$10 km s^{-1} (e.g. see [32, 33]). The main reasons for such conclusions are (a) low correlation of large ($\sim$6 rms) bursts of the ion saturation currents on different tips of the probe suggests that these bursts are not due to plasma blobs (e.g. see [34]) hitting the probe, as widely assumed in the tokamak plasma community, but due to collisions of high speed dust grains with the probe and (b) large ($\sim$100 μm in diameter) craters observed on the probe surface are consistent with the impact of high speed dust grains.

3. Basic processes of dust–plasma interactions in fusion plasmas

Here we discuss the basic processes of dust–plasma interactions in fusion devices and compare them with those in the rather well-developed area of dusty plasma experiments [35–37].

While dusty plasma experiments in most cases are performed with rather well characterized spherical dust grains, in fusion plasmas the shape, size and constituency of natural dust grains are not defined *a priori*. As a result, analysis of dust–plasma interactions in fusion plasmas is always approximate. But what is even more important is that due to the significant

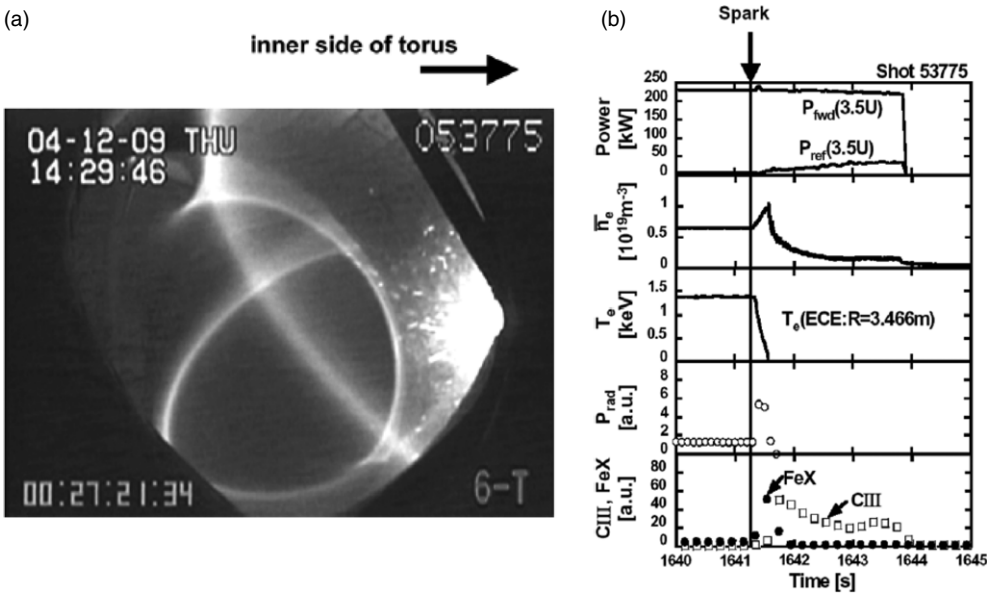

Figure 3. Termination of a long pulse discharge in LHD: (*a*) A spark observed on the inner side of a torus with the CCD camera, (*b*) corresponding time evolution of plasma parameters [9].

difference of plasma parameters in fusion devices and dusty plasma experiments, the accents of basic processes of dust–plasma interactions in these plasmas are shifted. In particular, hot, $T_i \sim T_e \sim 10$–$100\,\mathrm{eV}$, and rather dense, $n_e \sim 10^{12}$–$14\,\mathrm{cm}^{-3}$, practically fully ionized plasma at the edge of fusion devices heats the grain material to the temperatures $T_d \sim$ few $\times\, 10^3\,\mathrm{K}$, which is much higher than that in 'standard' weakly ionized dusty plasma conditions where $T_i \ll T_e \sim 1\,\mathrm{eV}$ and $n_e \gtrsim 10^{10}\,\mathrm{cm}^{-3}$. Therefore, dust in fusion plasmas quite quickly ablates/evaporates [28], unless it comes into some regions (e.g. the private region in a tokamak) with more relaxed plasma parameters.

In the case where the vapor does not affect the interactions of plasma electrons and ions with the grain, the processes of grain–plasma interactions in fusion devices can be described with the models developed for the study of dusty plasma (e.g. see [35–37] and the references therein), although with some corrections caused by the magnetic field effects. Here we briefly review the main results. For a typical strength of the magnetic field, B, in magnetic fusion devices, $B \sim 3\,\mathrm{T}$, plasma temperature $T = T_i \sim T_e \sim 10\,\mathrm{eV}$ and density $n_e \sim 10^{13}\,\mathrm{cm}^{-3}$ the ion, ρ_{Li}, and electron, ρ_{Le}, Larmor radii are respectively $\sim 100\,\mu\mathrm{m}$ and $\sim 1\,\mu\mathrm{m}$, while the Debye length, λ_D, is $\sim 10\,\mu\mathrm{m}$. Thus, for the grain with characteristic size $R_d \sim 1\,\mu\mathrm{m}$ we find that $\rho_{Li} > \lambda_D > R_d$ and the impact of the magnetic field on ion–grain interactions in many cases may be neglected. Although the electron–grain interactions will be somewhat altered by the magnetic field, due to the quasi-static nature of these interactions, the effect of the magnetic field on the charging will be modest. Then, neglecting all other possible mechanisms of dust charging, we come to the conclusion that is typical for dusty plasma: the grain is negatively charged and the charge number Z_d can be estimated as follows:

$$Z_d \sim \Lambda_Z R_d T/e^2, \tag{1}$$

where $\Lambda_Z \sim 3$ is the numerical coefficient which depends somewhat on the details of plasma and dust parameters. For $R_d \sim 1\,\mu\mathrm{m}$ and $T \sim 10\,\mathrm{eV}$ we find $Z_d \sim 10^4$. We note that due to the rather high plasma density, the charging time of dust in fusion plasmas is very short

$\sim 10^{-8}$ s [38]. Other possible mechanisms of dust grain charging in fusion devices are related to the thermionic and secondary electron emissions, as well as to the effects of both radioactivity and radiation. For the operational conditions of fusion devices the last two effects can be important for dust charging only in some remote regions with very weak (if any) plasmas. In contrast, the thermionic emission plays a very important role in fusion plasmas because of a large heat flux and, correspondingly, high temperature of dust material. Moreover, the thermionic emission makes the charge more positive which increases the energy flux to the grain. As a result of this positive feedback, the thermal instability of grain energy balance can occur [39].

While the interactions of the millimeter size pellets with fusion plasmas can cause relatively small but significant temperature variation within the grain, resulting, in particular in the 'rocket' effect (e.g. see [40] and the references therein), the temperature distribution within a much smaller μm size dust grain in most cases is practically uniform and its magnitude T_d is determined by the energy balance equation. In most regions of fusion devices the heating of dust is due to energy flux carried to the grain by plasma particles (including potential energy, which is realized in the process of plasma recombination at the grain). The heating due to plasma radiation usually is not important. We note that the roles of neutrals in both dust heating and cooling processes in fusion devices are relatively small due to practically complete ionization of neutrals. However, in so-called detached divertor regimes, the contribution of neutrals is sizable. The cooling of dust grains is associated with thermal radiation and dust ablation. Due to the fact that the size of the grain can be comparable to the typical wavelength of thermal radiation, the radiating power can significantly depart from the Stefan–Boltzmann scaling (e.g. [41]).

By solving coupled charging and energy balance equations one can find both equilibrium charge and steady-state temperature of dust as well as erosion/deposition rates that account for both sputtering and ablation as well as sticking of impurity ions to the dust. For typical edge plasma density $n_e \sim 3 \times 10^{13}\,\mathrm{cm}^{-3}$ and temperature $T_e \sim 30\,\mathrm{eV}$, we have $-\mathrm{d}R_d/\mathrm{d}t \sim 100\,\mu\mathrm{m\,s}^{-1}$ [28]. So that the μm size dust particle lifetime, τ_{lt}, appears to be about $\sim 10^{-2}\,\mathrm{s}^{-1}$. However, in low temperature plasma containing significant concentrations of intrinsic impurities (e.g. detached divertor plasmas, afterglow plasmas after discharge termination or disruption, and parasitic plasmas that occur in 'shadow' regions in some tokamaks) dust can grow.

Let us now discuss the forces acting on the dust grains in fusion plasmas. Analysis performed in [38] demonstrated that for $\sim\mu$m size grain, the main force is the plasma–dust particle friction force

$$\vec{F}_{\mathrm{fric}} = \varsigma_F \pi R_d^2 M_i n_e V_{Ti} (\vec{V}_p - \vec{V}_d), \tag{2}$$

where $\vec{V}_d$ and $\vec{V}_p$ are the plasma and dust grain velocities, M_i and V_{Ti} are the plasma ion mass and thermal speed and $\varsigma_F \sim 10$ is a numerical factor, which depends on dust charge and plasma parameters [36, 37]. The reason for the domination of the friction force is a strong plasma flows existing at the edge of fusion devices. Such flows, with Mach number $M \sim 1$, are formed due to a natural plasma recycling process when plasma in the SOL flows to material surfaces along the magnetic field lines, neutralizes there and then these neutrals come back into the plasma and are ionized there closing the recycling loop. Since the toroidal magnetic field in a tokamak is much stronger than the poloidal one, this flow mainly goes in toroidal directions. Moreover, due to the helical structure of the magnetic field lines, the flows in the outer and inner divertors have opposite toroidal directions.

The electric force, $\vec{F}_{\rm E} = Z_{\rm d} e \vec{E}$, is important mainly within a rather narrow, $\sim\rho_{\rm Li}$, sheath layer near material surfaces. This can be shown by comparison with the magnitudes of the electric and friction forces. Using estimate (1) and equation (2), we find

$$\frac{F_{\rm E}}{F_{\rm fric}} \sim \frac{1}{\varsigma_{\rm F} M} \frac{\lambda_{\rm D}^2}{R_{\rm d} L_\varphi} \frac{e\Delta\varphi}{T}, \tag{3}$$

where $\Delta\varphi$ is the variation of the effective electrostatic potential and L_φ is the characteristic length of the potential variation. In edge plasmas far from the wall, a strong radial variation $e\Delta\varphi \sim T$ occurs at $L_\varphi \sim 1\,$cm. Then, recalling that $\lambda_{\rm D} \sim 10\,\mu$m, from equation (3) we find that in practice $F_{\rm E} \ll F_{\rm fric}$ for $R_{\rm d} \sim 1\,\mu$m and only nano-scale dust particles experience a significant impact of the electric force.

For a μm size grain, the gravity, the magnetic and the rocket forces are only important in the regions with small Mach number of plasma flow. It is also easy to show that in tokamak plasma the impact of Lorentz force on μm scale particle motion is negligible, but for ~nm size dust particles it should be taken into account.

Let us now use the corresponding momentum balance equation for dust and estimate the speed, which a dust particle can reach from acceleration by the friction force. Considering that a strong plasma flow exists only within some particle path length, $L_{\rm d}$, from the momentum balance equation we find

$$V_{\rm d} \sim ((3/2)\varsigma_{\rm F} n_{\rm e} {\rm TML}_{\rm d}/(\rho_{\rm d} R_{\rm d}))^{1/2}, \tag{4}$$

which for typical dust and plasma parameters and for $L_{\rm d} \sim 10\,$cm gives $V_{\rm d} \sim 3 \times 10^4\,{\rm cm\,s^{-1}}$ [38]. Interestingly, due to opposite toroidal directions of plasma flows in the outer and inner divertors, which we mentioned before, the dust particles propelled by the friction force also are predicted to fly in opposite toroidal directions in the outer and inner divertors [42]. It seems that both experimental observations and the results of numerical modeling, which will be discussed later, support this simple argument.

Dust particles, being accelerated to high speed by the friction force, may not be confined anymore in the plasma volume by the sheath potential. Indeed, comparing dust kinetic energy, $E_{\rm d}^{\rm (kin)}$, determined by the speed from equation (5) to the potential barrier at the sheath, $E_{\rm d}^{\rm (pot)}$, it is easy to show that dust grain will go through the sheath even being negatively charged to the charge number given by expression (1). From equations (1) and (4) we find

$$\frac{E_{\rm d}^{\rm (kin)}}{E_{\rm d}^{\rm (pot)}} \sim \frac{\varsigma_{\rm F} M}{4\Lambda_Z \Lambda_{\rm sh}} \frac{R_{\rm d} L_{\rm d}}{\lambda_D^2} \tag{5}$$

assuming that the magnitude of the sheath potential is $\sim\Lambda_{\rm sh} T/e$, where $\Lambda_{\rm sh} \sim 3$ is the numerical coefficient. From equation (5) we see that for all practical parameters the kinetic energy of accelerated dust grain exceeds the sheath potential barrier by orders of magnitude. As a result, the collisions of dust particles with the wall surfaces become an important ingredient of dust dynamics in tokamak plasma.

Indeed, a dust particle, accelerated up to a few $100\,{\rm m\,s^{-1}}$ hitting the wall can lose significant kinetic energy, chip off small bits of the wall material or be fragmented itself. Such avalanche-like generation of dust can be very dangerous for both plasma performance and the safety of ITER.

The simulations of dust–wall collisions performed with the LS-DYNA, the commercial finite element program for structural analysis, considered the collisions of spherical dust particles with a flat surface [43, 44]. At low speeds $\sim 100\,{\rm m\,s^{-1}}$ no significant damage to the wall occurs. Dust grains reflect from the wall with the restitution coefficient ~0.7 and can be partially destroyed on the collision. At high impact speed $\sim 1\,{\rm km\,s^{-1}}$ beryllium dust

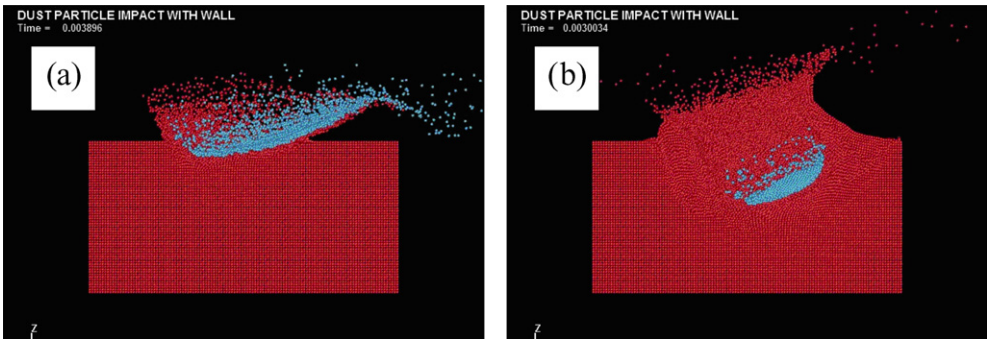

Figure 4. Simulated impact of a beryllium (*a*) and a tungsten (*b*) dust particle of radius 0.5 μm on a beryllium wall at speed 1 km s^{-1} and angle 45° to the normal wall [44].

is completely destroyed upon colliding, forming a cone of debris material injected into the plasma, figure 4(*a*). At the same speed the tungsten dust causes significant damage to the wall, forming a large crater at the wall, figure 4(*b*).

So far we have not considered any internal motion of the dust grain. Meanwhile, the spinning of dust particles has been observed in different environments ranging from laboratory to astrophysical plasmas [45]. The mechanisms leading to the spinning of dust particles can be associated with: dust–wall collisions, shear of the plasma flow; synergy of the plasma flow and asymmetry in the dust shape; synergy of the effects of the electric field, plasma flow with velocity, and electric dipole caused by the plasma flow; gyro-motion of magnetized ions striking the grain and some others. It is plausible that the dust grain fragmentation in tokamaks, seen from time to time with cameras, can be due to large mechanical stresses associated with dust spinning.

Our previous estimates of dust–plasma interactions including charging, heat fluxes to the grain, etc are based on orbit motion limited (OML) theory. However, high dust temperature causes intense ablation of the grain material and the presence of the vapor can significantly alter the interactions of plasma with the dust grain because the vapor can shield the grain from the plasma in a manner somewhat similar to that in pellet–plasma interactions [40]. As a crude estimate of the parameter range where one can expect a significant impact of the vapor, we can consider the effects of both ion–vapor collisions and electron impact ionization of the vapor. Vapor density can be found from the grain energy balance equation taking into account grain heating by the plasma and cooling by radiation loss and evaporation. Then we find that from rather 'large' dust grains, $R_d \gtrsim 30$–$100\,\mu$m, plasma–vapor interactions become important and standard OML theory and corresponding numerical modeling cannot be used.

However, the vapor issue is important not only for the physics of dust–plasma interactions, but also for the interpretation of experimental data. In particular, the interpretation of the camera images: what do we actually see on the camera? Is it the image of the grain due to the grain thermal radiation or it is the image coming from the plume formed by grain ablation and caused by the electron impact excitation of plume neutrals and ions? In order to get an idea about relative magnitudes of thermal radiation from the grain and visible line radiation from the plume we use the following estimates. A neutral impurity atom, which appears in hot plasma becomes ionized and simultaneously radiates in visible light. It is possible to introduce the energy E_{vis}, which will be radiated by one impurity atom/ion before it will be completely stripped of the electrons and practically stops to radiate (we assume low-Z impurity and relatively hot plasma). The total visible line radiation intensity from the plume, W_{plume}, in our case is proportional

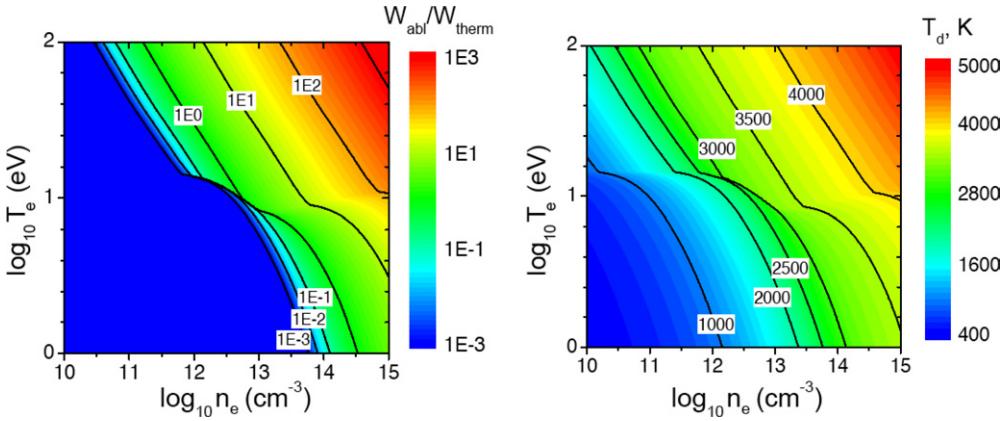

Figure 5. Contour plots of the ratio of $W_{\rm abl}/W_{\rm therm}$ and the temperature $T_{\rm d}$ as functions of plasma density and temperature.

to the ablation rate and, therefore, can be estimated as $W_{\rm plume} = (E_{\rm vis}/E_{\rm v})W_{\rm abl}$, where $W_{\rm abl}$ is the grain cooling power due to ablation and $E_{\rm v}$ is the evaporation energy. Then the ratio of visible line radiation from the plume to the thermal radiation from the grain, $W_{\rm therm}$, can be written as $W_{\rm plume}/W_{\rm therm} = (E_{\rm vis}/E_{\rm v})(W_{\rm abl}/W_{\rm therm})$, where both thermal radiation from the grain, $W_{\rm therm}$, and $W_{\rm abl}$ can be found from the energy balance of the grain, while $E_{\rm vis}$ can be obtained from the analysis of the radiation and ionization rates. Using the ADAS package we find that for electron temperature $\sim$10 eV and density $\sim 10^{13}$ cm^{-3} each injected atom of carbon will radiate $E_{\rm vis} \sim 100$ eV. It gives $E_{\rm vis}/E_{\rm v} \sim$ 10–30 (recall that at high heat load the ablation goes in cluster forms, which reduces effective $E_{\rm v}$ from $\sim$7 to $\sim$3 eV). The ratio of $W_{\rm abl}/W_{\rm therm}$ and the temperature $T_{\rm d}$, calculated with the DUSTT code, are shown in figure 5. As a result, we find that truly visible thermal radiation from the grain ($T_{\rm d} \gtrsim 1000$ K) prevails only within a rather narrow parameter range of plasma with very low density and temperature while in the rest of the edge plasma and, in particular, in some proximity to the separatrix plume radiation dominates.

4. Modeling of dust dynamics and transport in magnetic fusion devices

Modeling of dust in realistic tokamak conditions requires the development of rather complex numerical codes incorporating all aspects of dust–plasma and dust–wall interactions physics. In addition, the code needs the background plasma parameters, which can be provided either from some database or from plasma transport codes such as UEDGE [46] and SOLPS [47]. At this moment, two codes aimed at dust modeling in tokamaks are under development: the DTOKS code [48] and the more mature DUSTT code [28, 49]. Both codes solve the 3D equation of motion of dust particles coupled to dust charging and dust energy and mass balance models and both ignore the perturbations of background plasma parameters by individual grains as well as the grain–grain interactions.

In the DUSTT code the charging processes including thermionic and secondary electron emissions from dust particles are taken into account, which can result in the positively charged dust grains. Models for dust charging as well as particle and energy fluxes to the dust due to plasma, which are used in DUSTT, are valid for positive and negative dust charges and an arbitrary Mach number of the plasma flow (see [28, 49] for details). The generalization of

the radiation cooling of dust particles was introduced in the DUSTT code, which takes into account the dependences of the emissivity of small grains on their radius and both the optical properties and temperature of the grain's material (see [41]). A solid/liquid phase transition was implemented for non-carbon dust particles that takes into account the specific heat of dust material melting/solidification in the dust energy balance and different mechanical and thermo-physical properties of solid and molten dust material (see [50]). The statistical mode of the DUSTT code was developed such that, in addition to tracking of individual dust particle trajectories it allows the simulation of volumetric distributions of dust parameters in tokamaks, including calculations of averaged dust flux toward the core plasma.

The DUSTT code was intensively used in the last few years for both modeling of the dynamics of individual grains and comparison with experimental observations with fast cameras, as well as for the modeling of statistical properties of dust and comparison with statistical data coming from dust observations with a laser scattering technique.

The study of individual dust particle trajectories [28, 49] confirmed predictions [38] of the leading role of the friction force, which can accelerate dust in the toroidal direction to the speed $\sim$ several 100 m s^{-1}, which results in a strong impact of the effective centrifugal force on dust dynamics causing a predominant sweep of dust toward the outer wall and dust–wall collisions. Moreover, in agreement with early assessment [42] and experimental observations, the toroidal directions of dust motion in inner and outer divertors are often opposite due to opposite flows of plasma, which is caused by the interplay of natural plasma recycling and the helical structure of the magnetic field lines. Also, numerical modeling demonstrates an important role of dust–wall collisions, causing the scattering of the grain and mass and kinetic energy loss. Also, practically all particles coming to the separatrix show a jump in the charge from negative to positive [28], triggered by thermionic current. The tracks of dust particles experimentally observed with two fast cameras in the NSTX tokamak [21] were compared with simulated trajectories of particles with fitted initial conditions. The results show qualitative agreement between the simulated and experimentally observed trajectories. The fitting of the track's initial conditions allows us to estimate the recorded dust size roughly as $\sim$10 μm [21].

Statistical properties of dust in tokamak plasmas, such as the spatial profiles of dust number density, radius, temperature, charge and velocities in the plasma volume were simulated using the statistical mode of the DUSTT code. We notice that similar to the experimental observations [17, 18], the simulated dust density at the outer SOL is about one order lower than that in the divertor region due to the larger dust source in the divertor and more benign divertor plasma conditions.

It was also shown that penetration of neutral carbon associated with dust ablation into the hot plasma is much deeper than the penetration of carbon atoms and molecules sputtered from the walls. Deeper penetration of impurity can stimulate the divertor detachment. To model the effect of dust on detachment, the DUSTT code in conjunction with the UEDGE package were used [43]. Firstly we calculate with UEDGE the plasma profiles only for wall sputtered impurities launched as neutral atoms (figure 6(*a*)). Then, we use these plasma parameter profiles to calculate with DUSTT the neutral impurity penetration and neutral impurity source assuming that $\xi_{\mathrm{d}} = 8\%$ of impurity influx is launched into plasma as 1 μm dust particles. After that we use this neutral impurity source and again run UEDGE to calculate new steady-state plasma profiles displayed in figure 6(*b*). Comparing figures 6(*a*) and (*b*) one sees a dramatic impact of dust on the outer leg detachment. We note, however, that these results just highlight the trends and are not completely self-consistent because we do not iterate between dust penetration through edge plasma and impact of neutral impurity, partly related to dust ablation, on plasma parameter variation.

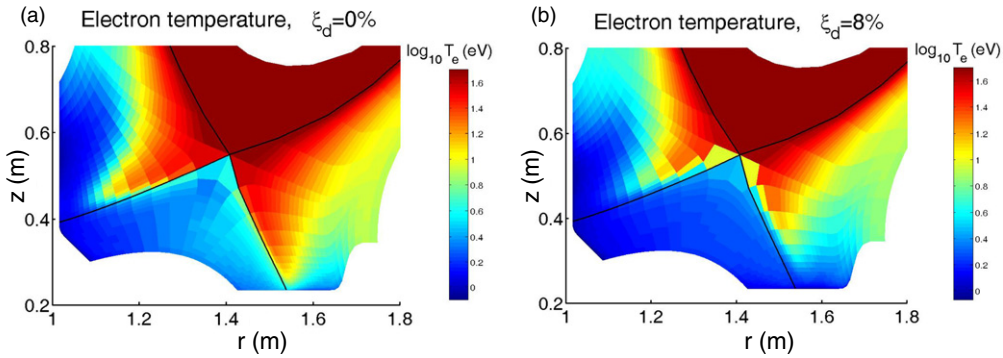

Figure 6. Impact of dust on divertor detachment in DIII-D plasma [43].

5. Conclusions

In recent years significant progress has been achieved in the understanding of the physics of dust in magnetic fusion plasmas. While just a few years ago the main experimental technique was the analysis of dust in fusion devices during vessel entries, today laser scattering, multiple fast cameras and some other diagnostics are successfully used for the *in situ* study of dust. The processes playing the most important roles in dust dynamics and transport in fusion plasmas were identified. Rather sophisticated 3D codes tracking dust in tokamak plasma and able to provide both the motion of the individual grain and statistics of the ensemble of the dust particle were developed and used for dust studies in current tokamaks and ITER. Comparison of code results with experimental data and applications of newly developed codes for the interpretation of dust measurements have become more common. In particular, good qualitative agreements were found between theoretical prediction, results of numerical modeling and experimental observations of the magnitude and directions of dust motion in tokamak divertors. Benchmarking of numerical codes and experimental observations is in progress (e.g. preliminary results of the comparison of the dust grain trajectory provided by multiple fast cameras with modeling with code DUSTT) and should provide some confidence in the physical models used for the description of dust–plasma interactions.

However, there are still some significant and crucial gaps in our understanding of dust in fusion plasmas. The most important ones seem to be: what physics dominates and what determines the rate of dust generation? To answer these questions, more detailed experimental data on *in situ* dust and wall monitoring are needed in conjunction with the development of theoretical and numerical models of dust generation.

References

[1] Winter J 1998 *Plasma Phys. Control. Fusion* **40** 1201
[2] Federici G *et al* 2001 *Nucl. Fusion* **41** 1967
[3] Rubel M *et al* 2001 *Nucl. Fusion* **41** 1087
[4] Sharpe J P, Petti D A and Bartels H-W 2002 *Fusion Eng. Des.* **63–64** 153
[5] Winter J 2004 *Plasma Phys. Control. Fusion* **46** B583
[6] Girard J-Ph *et al* 2007 *Fusion Eng. Des.* **82** 506
[7] Shimomura Y 2007 *J. Nucl. Mater.* **363–365** 467
[8] ITER Document ITER_D_2EJUVK
[9] Saito K *et al* 2007 *J. Nucl. Mater.* **363–365** 1323
[10] Carmack W J *et al* 2000 *Fusion Eng. Des.* **51–52** 477

[11] Sharpe J P *et al* 2001 *Fusion Technol.* **39** 1061
[12] Sharpe J P *et al* 2003 *J. Nucl. Mater.* **313–316** 455
[13] Bekris N *et al* 2005 *J. Nucl. Mater.* **337–339** 659
[14] Sharpe J P *et al* 2005 *J. Nucl. Mater.* **337–339** 1000
[15] Sasaki K *et al* 2007 *J. Nucl. Mater.* **363–365** 238
[16] Narihara K *et al* 1997 *Nucl. Fusion* **37** 1177
[17] West W P *et al* 2006 *Plasma Phys. Control. Fusion* **48** 1661
[18] West W P *et al* 2007 *J. Nucl. Mater.* **363–365** 107
[19] Maqueda R J and Wurden G A 1999 *Nuc. Fusion* **39** 629
[20] Counsell G F 2004 private communication
[21] Roquemore A L *et al* 2007 *J. Nucl. Mater.* **363–365** 222
[22] Rudakov D L *et al* 2007 *J. Nucl. Mater.* **363–365** 227
[23] Litnovsky A 2008 private communication
[24] Skinner C H *et al* 2008 *J. Nucl. Mater.* **376** 29
[25] Counsell G F *et al* 2006 *Rev. Sci. Instrum.* **77** 093501
[26] Chappuis Ph *et al* 2001 *J. Nucl. Mater.* **290–293** 245
[27] Masaki *et al* 2005 *J. Nucl. Mater.* **337–339** 553
[28] Smirnov R D *et al* 2007 *Plasma Phys. Control. Fusion* **49** 347
[29] Smirnov R D *et al* 2007 *Phys. Plasmas* **14** 112507
[30] Goodall D H J 1982 *J. Nucl. Mater.* **111–112** 11
[31] Lupschultz B *et al* 2005 Operational recovery from enormous amounts of titanium dust *ITPA Meeting of Divertor and SOL Physics Group (Tarragona, Spain, 4–7 July 2005)*
[32] Castaldo C *et al* 2007 *Nucl. Fusion* **47** L5
[33] Ratynskaia S *et al* 2008 *Nucl. Fusion* **48** 015006
[34] Krasheninnikov S I 2001 *Phys. Lett.* A **283** 368
[35] Tsytovich V N 1997 *Phys.—Usp.* **40** 53
[36] Shukla P K and Mamun A A 2002 *Introduction to Dusty Plasma Physics* (Bristol: Institute of Physics Publishing)
[37] Fortov V E *et al* 2005 *Phys. Rep.* **421** 1
[38] Krasheninnikov S I *et al* 2004 *Phys. Plasmas* **11** 3141
[39] Nedospasov A V and Petrov V G 1983 *Sov. Phys.—Dokl.* **28** 293
[40] Milora S L *et al* 1995 *Nucl. Fusion* **35** 657
[41] Rosenberg M *et al* 2008 *J. Phys. D: Appl. Phys.* **41** 015202
[42] Krasheninnikov S I and Soboleva T K 2005 *Plasma Phys. Control. Fusion* **47** A339
[43] Krasheninnikov S I *et al* 2006 *21st IAEA Fusion Energy Conf. (Chengdu, China, 16–21 October 2006)* Paper TH/P6-18
[44] Smirnov R D *et al* 2008 Assessment of dust dynamics and transport in tokamak edge plasmas *18th Int. Conf. on Plasma Surface Interaction (Toledo, Spain, 26–30 May)*
[45] Sato N 2005 *New Vistas in Dusty Plasmas* ed L Boufendi *et al AIP Conf. Proc.* vol 799 (New York: American Institute of Physics) p 97
Hutchinson I H 2004 *New J. Phys.* **6** 43
Tsytovich V N *et al* 2003 *New J. Phys.* **5** 43
Tsytovich V and Vladimirov S 2004 *IEEE Trans. Plasma Sci.* **32** 659
Krasheninnikov S I *et al* 2007 *Phys. Lett.* A **361** 133
Krasheninnikov S I 2006 *Phys. Plasmas* **13** 114502
[46] Rognlien T D *et al* 1992 *J. Nucl. Mater.* **196–198** 34
[47] Schneider R *et al* 2006 *Contrib. Plasma Phys.* **46** 3
[48] Martin J D *et al* 2006 *33rd EPS Conf. on Plasma Physics (Rome, 19–23 June 2006)* vol 30I, (ECA) O-4.010
[49] Pigarov A Yu *et al* 2005 *Phys. Plasmas* **12** 122508
[50] Tanaka Y *et al* 2007 *Phys. Plasmas* **14** 052504